Medicinal Chemistry Research (2019) 28:2128–2141
https://doi.org/10.1007/s00044-019-02441-2

MEDICINAL CHEMISTRY RESEARCH

ORIGINAL RESEARCH

Synthesis and in silico and in vitro evaluation of trimethoxy-benzamides designed as anti-prion derivatives

Raissa A. Conceição[1] · Lucas M. Ascari[1] · Natália C. Ferreira[1,2] · Carolina F. Goes[1] · Carolina O. Matos[3] · Anderson S. Pinheiro[3] · Marina A. Alves[4] · Alessandra M. T. Souza[1] · Rodolfo C. Maia[5] · Byron Caughey[2] · Yraima Cordeiro[1] · Maria Letícia C. Barbosa[1,5]

Received: 18 March 2019 / Accepted: 4 September 2019 / Published online: 14 September 2019

Abstract

Transmissible spongiform encephalopathies (TSEs), also known as prion diseases, are neurodegenerative disorders which affect mammals, including the human species, and arise after the conversion of the monomeric cellular prion protein (PrP^{C}) into the aggregated scrapie form (PrP^{Sc}). There is no therapy to treat TSEs and the identification of compounds that bind PrP^{C}, preventing its conversion into PrP^{Sc}, is a viable therapeutic strategy. We designed and synthesized six novel trimethoxy-benzamide compounds as anti-prion drug candidates. Molecular docking analyses predicted that all the derivatives bind to a *hotspot* region located in the PrP globular domain with very similar spatial orientation and interaction mode. Although none of the analogs inhibited in vitro-aggregation of recombinant PrP (rPrP) in a cell-free conversion assay, the RT-QuIC, compound **8a** accelerated rPrP conversion into PrP^{Sc}-like species. STD-NMR and ITC analyses indicated that both **8a** and **8b** bind to $rPrP^{90–231}$. These analogs were toxic to PrP^{Sc}-infected cell lines, hence we could not assess their anti-prion activity by using this cellular approach, although this toxicity was cell line-dependent. These results point out that the 4-amino-quinoline trimethoxy-benzamide scaffold described herein represents a novel chemical pattern useful as a starting point for future structural optimization in the design of PrP ligands with improved affinity and safety profiles.

Keywords Prion protein · Anti-prion drug · Therapy · Anti-scrapie compounds · Molecular hybridization · Prion strains

Introduction

The term *prion*, coined by Stanley Prusiner, was originated from the expression *proteinaceous infectious particle* (Prusiner 1998), denoting its putative property of acting as an unusual causative infectious agent in the pathogenesis of transmissible spongiform encephalopathies (TSEs), also known as prion diseases (Prusiner 1998). TSEs comprise a collection of genetic, infectious, or sporadic neurodegenerative disorders that affect humans and other mammals and are triggered by the conversion of the native cellular prion protein (PrP^{C}) into its pathogenic, misfolded form, which is commonly referred as prion scrapie (PrP^{Sc}) (Caughey et al. 2009).

These authors contributed equally: Raissa A. Conceição, Lucas M. Ascari

Supplementary information The online version of this article (https://doi.org/10.1007/s00044-019-02441-2) contains supplementary material, which is available to authorized users.

✉ Yraima Cordeiro
yraima@pharma.ufrj.br

✉ Maria Letícia C. Barbosa
marialeticia@pharma.ufrj.br

[1] Faculty of Pharmacy, Federal University of Rio de Janeiro (UFRJ), Rio de Janeiro, RJ, Brazil

[2] Laboratory of Persistent Viral Diseases, Rocky Mountain Laboratories, National Institute of Allergy and Infectious Diseases, National Institutes of Health, Hamilton, MT, USA

[3] Department of Biochemistry, Institute of Chemistry, Federal University of Rio de Janeiro (UFRJ), Rio de Janeiro, RJ, Brazil

[4] Laboratory for the Support of Technological Development (LADETEC), Institute of Chemistry, Federal University of Rio de Janeiro (UFRJ), Rio de Janeiro, RJ, Brazil

[5] Laboratory of Evaluation and Synthesis of Bioactive Substances (LASSBio), Institute of Biomedical Sciences, Federal University of Rio de Janeiro (UFRJ), Rio de Janeiro, RJ, Brazil

The constitutive, α-helix-rich PrP^{C} is specially abundant in the nervous and immune systems and is typically located on the cell surface via a glycosyl-phosphatidyl inositol (GPI) anchor (Caughey et al. 2009). According to the protein-only hypothesis, the aberrant, β-sheet-rich PrP^{Sc} induces PrP^{C} misfolding and promotes the propagation and amplification of PrP^{Sc} aggregates, which, in turn, induce widespread neurotoxicity (Caughey et al. 2009). While PrP^{C} is protease-sensitive, PrP^{Sc} is partially protease-resistant and, for that reason, is also referred as PrP^{Res} (Prusiner 1998; Caughey et al. 2009).

The precise mechanism of transmission and propagation of TSEs is still controversial, especially regarding the potential involvement of cofactors assisting PrP^{C} to PrP^{Sc} conversion (Abid et al. 2010; Supattapone 2014; Macedo and Cordeiro 2017). In addition, evidences indicate that subversion of PrP^{C} normal function by PrP^{Sc} is a key process in the pathophysiology of TSEs (Westergard et al. 2007). In normal conditions, PrP^{C} is thought to play a physiological role as a scaffold protein in cell signaling (Linden 2017) and to take part in cell survival, cell differentiation, cell adhesion, Cu^{2+} homeostasis, synaptic transmission, myelin maintenance, and neuroprotection (Castle and Gill 2017).

Prion diseases are usually associated with long silent incubation periods, ranging from years to decades. However, when the clinical signs become detectable, disease usually progresses in a fast and aggressive manner, leading to severe disability and death (Prusiner 1998). Unfortunately, there is no effective therapy available in the clinics, highlighting the relevance of searching for novel alternatives for the treatment of TSEs.

Several promising bioactive compounds from different structural classes, like 4-amino-quinolines and trimethoxychalcones, have been described in the literature for their anti-prion effects in in vitro and/or in vivo assays. However, none of them have proven to be effective in preventing the progress of TSEs in clinical trials so far (reviewed in Cordeiro and Ferreira 2015; Forloni et al. 2013). Among the previously identified anti-prion drug candidates, some already approved drugs—e.g., quinacrine (**1**) (Geschwind et al. 2013), flupirtine (**2**) (Otto et al. 2004), and doxycycline (**3**) (Haïk et al. 2014)—stood out during preclinical studies, suggesting the possibility of their repositioning for TSE treatment (Fig. 1). However, these drugs were also not effective in further clinical stages of development (Forloni et al. 2013; Ghaemmaghami et al. 2014).

A *hotspot* region within PrP^{C} structure, which is susceptible to undergo conformational fluctuations, comprises specific amino acid residues, such as Asn159 at the α1–β2 loop; His187, Val189, Thr192, and Lys194 at the α2; and Glu196 at the α2–α3 loop (Langella et al. 2004; Kuwata et al. 2007). In an attempt to identify novel PrP^{C}-stabilizing ligands, one of the putative molecular mechanisms for small anti-prion molecules, these authors conducted in vitro, in silico, and in vivo assays and have reported the anti-prion activity of prototype GN8 (**4**) (Kuwata et al. 2007; Yamamoto and Kuwata 2009; Ishikawa et al. 2009) (Fig. 1).

Kuwata and coworkers reported that GN8 (**4**) was able to reduce the PrP^{Res} content in prion-infected cells and prolong the survival of TSE-infected mice. Using nuclear magnetic resonance (NMR) and computational simulations, this molecule was shown to interact with the *hotspot* region

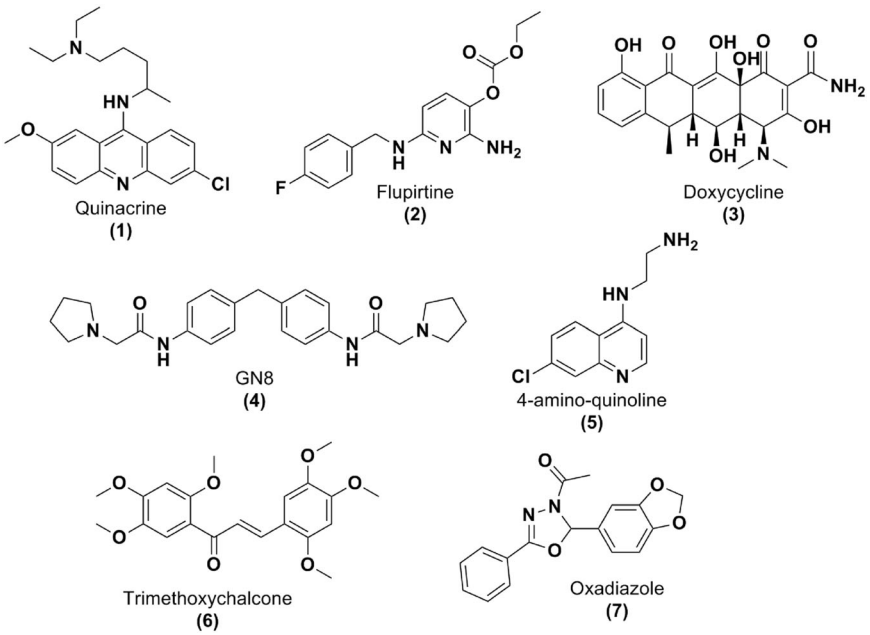

Fig. 1 Anti-prion prototypes previously described in the literature

within the major cavity of PrP globular domain. The reporting of this key *hotspot* pocket emphasized its relevance for the structural stabilization of PrP^C and thus offered the basis for further efforts in order to find novel anti-prion drug candidates (Hyeon et al. 2015; Ishibashi et al. 2016).

Our research group has contributed to this field with the description of anti-prion derivatives bearing different chemical scaffolds, including 4-amino-quinolines (Macedo et al. 2010), trimethoxy-chalcones (Ferreira et al. 2014, 2018), and oxadiazoles (Ferreira et al. 2014), as exemplified by compounds **5**–**7** depicted in Fig. 1. Herein we describe the synthesis and the in silico and in vitro evaluation of new trimethoxy-benzamide analogs, designed by molecular hybridization from the 4-amino-quinoline **5** and the trimethoxy-chalcone **6**, as novel anti-prion candidates (Fig. 2).

Material and methods

Chemistry

All commercially available reagents and solvents were used without further purification. Reactions were routinely monitored by thin-layer chromatography (TLC) in silica gel (F245 Merck plates), and the products were visualized with ultraviolet light (254 and 365 nm). ^1H and ^{13}C NMR spectra were determined in DMSO-d_6, D_2O, TFA-*d*, acetone-d_6, or $CDCl_3$ solutions using a Varian 400-MR (IPPN-UFRJ, BR) spectrometer. The chemical shifts are given in parts per million (δ) from solvent residual peaks, and the coupling constant values (J) are given in Hz. Signal multiplicities are represented by s (singlet), d (doublet), dd (double doublet), t (triplet), dt (double triplet), q (quadruplet), qu (quintuplet), m (multiplet) and/or br (broad signal). Saturation transfer

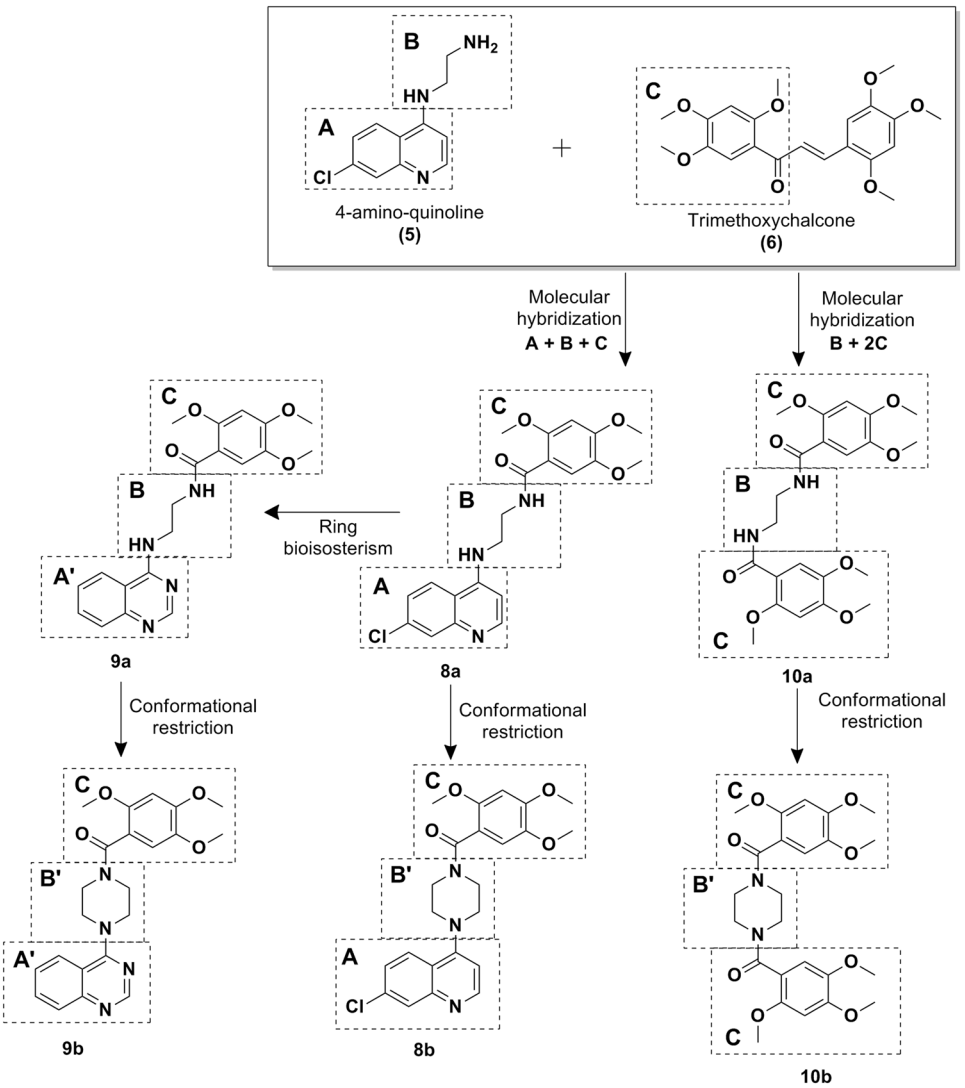

Fig. 2 Structural design of the target trimethoxy-benzamide analogs, designed by molecular hybridization from the 4-amino-quinoline **5** and the trimethoxy-chalcone **6**, as novel anti-prion candidates

difference NMR (STD-NMR) spectra were collected at 25 °C on a 600 MHz Bruker Avance III spectrometer equipped with a room temperature inverse-detection 5-mm TXI probe.

Mass spectra were obtained using a QExactive™ Hybrid Quadrupole Orbitrap Mass Spectrometer (Thermo Fisher Scientific, Waltham, USA) using electrospray ionization. High-resolution mass spectrometry (HRMS) data were obtained at the Laboratory for the Support of Technological Development of the Federal University of Rio de Janeiro (LADETEC-UFRJ, BR).

The purity of the testing compounds was determined by HPLC on a Shimadzu Prominence HPLC system (Shimadzu, Tokio, Japan) consisting of a vacuum degasser (DGU-20A5), a binary pump (LC-20AD), an autosampler (SIL-20A), UV/VIS Photodiode Array Detector (SPD-M20A) and fitted with a guard column (CLC G-ODS) and a Shimadzu (CLC-ODS, M) column (250 × 4.6 mm ID) running at room temperature. The mobile phase was prepared with Milli-Q water (A) and with acetonitrile (B) for the compounds **8a**, **8b**, **9b**, **10a**, and **10b**; and with Milli-Q water containing 0.1% formic acid (A) and with acetonitrile (B) for the compound **9a**. Isocratic elution was performed with 1:1 or 6:4 acetonitrile:water, at a flow rate set at 1 mL/min, and a 20 µL injection volume was used. The detection was carried out in the range of 294–330 nm wavelengths.

All testing compounds, i.e., trimethoxy-benzamide derivatives (**8a**, **8b**, **9a**, **9b**, **10a**, and **10b**), were characterized by ^{1}H and ^{13}C NMR and HRMS, showing spectral data according to the assigned structures. Compounds **8a**, **8b**, **9a**, **9b**, **10a**, and **10b** presented >95% purity, as assessed by HPLC.

We used the following recombinant PrP (rPrP) constructs: hamster rPrP$^{23–231}$, hamster rPrP$^{90–231}$, and mouse rPrP$^{90–231}$. They were expressed in *E. coli* and purified by nickel affinity chromatography and refolded in-column, as previously described (Wilham et al. 2010).

Synthesis of 2,4,5-trimethoxybenzoyl chloride (14)

In a 100 mL flask, 2,4,5-trimethoxybenzoic acid **15** (0.50 g, 2.36 mmol) was dissolved in dichloromethane (50 mL). Next, oxalyl chloride (0.66 g, 477 µL, 5.21 mmol) and 2 drops of dimethylformamide were added. The resulting solution was stirred at room temperature for 2–4 h and the end of the reaction was detected by TLC (70% ethyl acetate: 30% hexane). The desired acyl-chloride **14** was isolated after solvent evaporation under reduced pressure with a yield of 100% and was used as crude product for the synthesis of benzamide derivatives **10a**, **10b**, **13a**, and **13b** (Scheme 2c).

Synthesis of trimethoxy-benzamide intermediates 13a and 13b

A solution of acyl-chloride **14** (0.544 g, 2.36 mmol) in dichloromethane (50 mL) was slowly added dropwise into a 250 mL flask containing a 10 eq solution (23.6 mmol) of the corresponding amine (ethylenediamine or piperazine) in 20 mL of dichloromethane, under constant stirring at room temperature. The resulting reaction mixture was stirred at room temperature for around 20 min, when the end of the reaction was detected by TLC (10% methanol: 90% dichloromethane). The obtained trimethoxy-benzamide intermediates were isolated by the addition of 50 mL distilled water, followed by extraction in a separating funnel. These intermediates could be easily purified by acid–base extraction. Initially, basic derivatives **13a** and **13b** were extracted from the organic layer with an aqueous solution of HCl (pH = 3). Afterwards, pH of the aqueous layer was adjusted to neutrality and the pure benzamides **13a** and **13b** were extracted back to the organic layer. The final organic layers containing derivatives **13a** and **13b** were then dried over anhydrous sodium sulfate, filtered, and concentrated under reduced pressure (Scheme 2d).

***N*-(2-aminoethyl)-2,4,5-trimethoxybenzamide (13a)** Beige oil; yield: 75%; ^{1}H NMR (DMSO-d_6, 400 MHz): $\delta = 2.74$ (2H, t, $J = 6.4$ Hz, C$\underline{H}_2$NH$_2$), 3.33 (2H, q, $J = 5.96$ Hz, CONHC$\underline{H}_2$), 3.63 (2H, br, N$\underline{H}_2$), 3.72 (3H, s, ArOC$\underline{H}_3$), 3.85 (3H, s, ArOC$\underline{H}_3$), 3.91 (3H, s, ArOC$\underline{H}_3$), 6.74 (1H, s, H-3), 7.44 (1H, s, H-6), 8.29 (1H, br, CON$\underline{H}$); ^{13}C NMR and APT (DMSO-*d6*, 100 MHz): $\delta = 40.6$ (C$\underline{H}_2$), 41.0 (C$\underline{H}_2$), 55.0 (CH$_3$, ArO$\underline{C}$H$_3$), 55.9 (CH$_3$, ArO$\underline{C}$H$_3$), 56.7 (CH$_3$, ArO$\underline{C}$H$_3$), 97.7 (CH, C-3), 112.9 (C, C-1), 113.6 (CH, C-6), 142.4 (C, C-2), 152.1 (C, C-5), 152.5 (C, C-4), 164.5 (C, $\underline{C}$=O).

Piperazin-1-yl(2,4,5-trimethoxyphenyl)methanone (13b) Beige oil; yield: 95%; ^{1}H NMR (DMSO-d_6, 400 MHz): $\delta =$ 2.61 (2H, br, HNC$\underline{H}_2$R), 2.72 (2H, t, $J = 4.9$ Hz, HNC$\underline{H}_2$R), 3.08 (2H, br, CONC$\underline{H}_2$R), 3.52 (2H, br, CONC$\underline{H}_2$R), 3.69 (3H, s, ArOC$\underline{H}_3$), 3.77 (3H, s, ArOC$\underline{H}_3$), 3.81 (3H, s, ArOC$\underline{H}_3$), 6.71 (1H, s, H-3), 6.75 (1H, s, H-6); ^{13}C NMR and APT (DMSO-*d6*, 100 MHz): $\delta = 42.1$ (C$\underline{H}_2$), 45.2 (C$\underline{H}_2$), 45.7 (C$\underline{H}_2$), 47.4 (C$\underline{H}_2$), 55.9 (CH$_3$, ArO$\underline{C}$H$_3$), 55.9 (CH$_3$, ArO$\underline{C}$H$_3$), 56.3 (CH$_3$, ArO$\underline{C}$H$_3$), 97.9 (CH, C-3), 112.0 (CH, C-6), 116.4 (C, C-1), 142.8 (C, C-2), 149.5 (C, C-5), 150.3 (C, C-4), 166.5 (C, $\underline{C}$=O).

Synthesis of the designed bis-trimethoxy-benzamide analogs 10a and 10b

The acyl-chloride **14** (0.110 g, 0.48 mmol) was initially dissolved in dichloromethane (5 mL) and stirred at room

temperature, followed by the gradual addition of 1–4 equivalents of the corresponding amines (ethylenediamine or piperazine) until the end of the reaction, detected by TLC. The work-up consisted of adding 10 mL of dichloromethane to the flask and then washing the organic phase with 10 mL of 10% HCl aqueous solution. Then, the organic phase was dried with sodium sulfate and concentrated under reduced pressure. The resulting residues were purified in chromatographic columns, using dichloromethane as eluent, to provide the desired bis-trimethoxybenzamide analogs **10a** and **10b** (Scheme 2e).

***N,N′*-(ethane-1,2-diyl)bis(2,4,5-trimethoxybenzamide) (10a)** White solid; yield: 82%; ^{1}H NMR (DMSO-d_6, 400 MHz) (Fig. S1): $\delta = 3.48$ (4H, br $NC\underline{H}_2$), 3.71 (6H, s, $ArOC\underline{H}_3$), 3.84 (6H, s, $ArOC\underline{H}_3$), 3.88 (6H, s, $ArOC\underline{H}_3$), 6.72 (2H, s, H-3 and H-3′), 7.46 (2H, s, H-6 and H-6′), 8.30 (2H, s, CONH); ^{13}C NMR (DMSO-d_6, 100 MHz) (Fig. S2): $\delta = 39.3$ ($\underline{C}H_2$), 55.9 (CH_3, $ArO\underline{C}H_3$), 55.9 (CH_3,$ArO\underline{C}H_3$), 56.5 (CH_3,$ArO\underline{C}H_3$), 97.8 (CH, C-3), 112.7 (C, C-1), 113.8 (CH, C-6), 142.5 (C, C-2), 152.2 (C, C-5), 152.6 (C, C-4), 164.7 (C, $\underline{C}$=O); ^{1}H NMR ($CDCl_3$, 400 MHz): $\delta = 3.69$ (2H, br, $C\underline{H}_2$), 3.70 (2H, br $C\underline{H}_2$), 3.89 (6H, s, $ArOC\underline{H}_3$), 3.90 (6H, s, $ArOC\underline{H}_3$), 3.92 (6H, s, $ArOC\underline{H}_3$), 6.49 (2H, s, H-3 and H-3′), 7.75 (2H, s, H-6 and H-6′), 8.18 (2H, s, CONH); ^{13}C NMR and APT ($CDCl_3$, 100 MHz): $\delta = 39.8$ ($\underline{C}H_2$), 56.2 (CH_3, $ArO\underline{C}H_3$), 56.3 (CH_3, $ArO\underline{C}H_3$), 56.7 (CH_3, $ArO\underline{C}H_3$), 96.6 (CH, C-3), 113.0 (C, C-1), 114.2 (CH, C-6), 143.3 (C, C-2), 152.5 (C, C-5), 152.9 (C, C4), 165.8 (C, $\underline{C}$=O); HRESIMS *m/z* (Fig. S3): $[M+Na]^+$: 471.17368 $C_{22}H_{28}N_2NaO_8$ (calcd. 471.17378).

Piperazine-1,4-diylbis((2,4,5-trimethoxyphenyl)methanone) (10b) White solid; yield: 87%; ^{1}H NMR (DMSO-d_6, 400 MHz) (Fig. S4): $\delta = 3.16$ (4H, br, $C\underline{H}_2$), 3.54 (4H, br, $C\underline{H}_2$), 3.67–3.82 (18H, m, $ArOC\underline{H}_3$), 6.67 (1H, s, H-3), 6.73 (1H, s, H-3′), 6.80 (1H, s, H-6 and H-6′); ^{13}C NMR (DMSO-d_6, 100 MHz) (Fig. S5): $\delta = 40.0$ ($\underline{C}H_2$), 40.4 ($\underline{C}H_2$), 45.2 ($\underline{C}H_2$), 45.6 ($\underline{C}H_2$), 53.8 (CH_3, $ArO\underline{C}H_3$), 54.7 (CH_3, $ArO\underline{C}H_3$), 54.9 (CH_3, $ArO\underline{C}H_3$), 55.0 (CH_3, $ArO\underline{C}H_3$), 55.0 (CH_3, $ArO\underline{C}H_3$), 96.5 (CH, C-3), 96.6 (CH, C-3′), 110.9 (CH, C-6), 111.0 (CH, C-6′), 114.7 (C, C-1), 114.7 (C, C-1′), 141.5 (C, C-2), 141.6 (C, C-2′), 148.3 (C, C-5), 148.3 (C, C-5′), 149.2 (C, C-4), 149.2 (C, C-4′), 165.3 (C, $\underline{C}$=O); HRESIMS *m/z* (Fig. S6): $[M+Na]^+$ 497.18888 $C_{24}H_{30}N_2NaO_8$ (calcd. 497.18943).

Synthesis of the designed 7-chloro-4-amino-quinoline analogs 8a and 8b

In a 50 mL flask equipped with a reflux condenser, the 4,7-dichloroquinoline **11** (80 mg, 0.40 mmol) was dissolved in 8 mL of isopropyl alcohol. Next, 1.1 equivalents of the

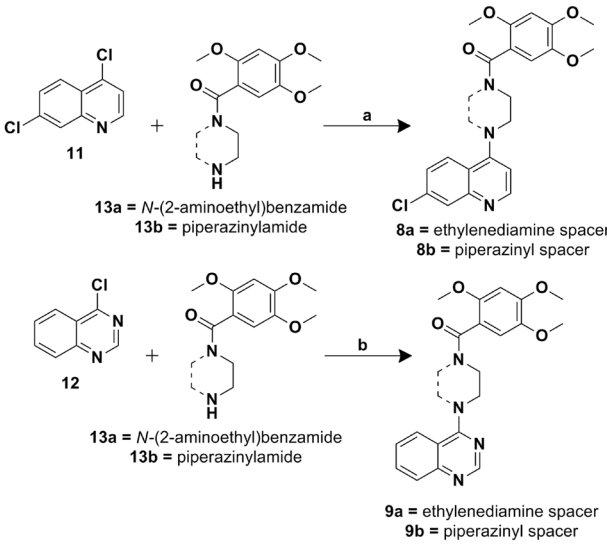

Scheme 1 Reagents and conditions: (**a**) isopropyl alcohol, 82 °C, 48–72 h, 45–56%; (**b**) isopropyl alcohol, Et_3N, 82 °C, 48–72 h, 54–72%

corresponding benzamide intermediate (**13a** or **13b**) were added. The resulting reaction mixture was stirred and heated at 82 °C until completion of the reaction, verified by TLC (10% methanol: 90% dichloromethane). The resulting precipitate was directly isolated by vacuum filtration (Scheme 1a).

***N*-(2-((7-chloroquinolin-4-yl)amino)ethyl)-2,4,5-trimethoxybenzamide (8a)** Beige powder; yield: 45%; ^{1}H NMR (D_2O, 600 MHz) (Fig. S7): $\delta = 3.51$ (3H, s, $ArOC\underline{H}_3$), 3.52 (3H, s, $ArOC\underline{H}_3$), 3.61 (2H, t, $C\underline{H}_2$), 3.68 (2H, t, $C\underline{H}_2$), 3.72 (3H, s, $ArOC\underline{H}_3$), 6.41 (1H, s, H3′), 6.63 (1H, d, *Jortho* = 7.4 Hz, H-3), 6.87 (1H, s, H6′), 7.46 (1H, d, *Jortho* = 9.3 Hz, *Jmeta* = 2 Hz, H-6), 7.89 (1H, d, *Jortho* = 7.4 Hz, H-2), 7.90 (1H, d, *Jortho* = 9,3 Hz, H-5); ^{1}H NMR (TFA, 400 MHz) (Fig. S8): $\delta = 4.36$ (13H, m, $C\underline{H}_2$ and $ArOC\underline{H}_3$), 7.13 (1H, s, H-3′), 7.23 (1H, s, H-6′), 7.96 (1H, br, H-3), 8.03 (1H, br, H-6), 8.21 (1H, s, H-8), 8.53 (1H, br, H-5), 8.63 (1H, br, H-2); ^{13}C NMR (TFA, 100 MHz) (Figs. S9 and S10): $\delta = 39.6$ ($\underline{C}H_2$), 43.8 ($\underline{C}H_2$), 55.8 (CH_3, $ArO\underline{C}H_3$), 56.5 (CH_3, $ArO\underline{C}H_3$), 56.7 (CH_3, $ArO\underline{C}H_3$), 96.8 (CH, C-3′), 98.3 (CH, C-6′), 106.6 (C, C-1′), 115.4 (CH, C-3), 119.6 (C, C-4a), 123.6 (CH, C-6), 129.4 (CH, C-5), 138.5 (CH, C-8), 142.2 (C, C-7), 142.6 (C, C-2′), 143.3 (CH, C-2), 156.6 (C, C-5′), 156.9 (C, C-4′), 157.2 (C, C-8a), 171.1 (C, C-4), 181.4 (C, $\underline{C}$=O); HRESIMS *m/z* (Fig. S11): $[M+H]^+$ 416.13677 $C_{21}H_{23}ClN_3O_4$ (calcd. 416.13716).

(4-(7-chloroquinolin-4-yl)piperazin-1-yl)(2,4,5-trimethoxyphenyl)-methanone (8b) Beige powder; yield: 56%; ^{1}H NMR (D_2O, 400 MHz) (Fig. S12): $\delta = 3.62$ (2H, br,

RNC$\underline{H}_2$R), 3.75 (3H, s, ArOC$\underline{H}_3$), 3.81 (3H, s, ArOC$\underline{H}_3$), 3.83 (3H, s, ArOC$\underline{H}_3$), 3.97 (2H, br, RNC$\underline{H}_2$R), 6.68 (1H, s, H-3′), 6.88 (1H, s, H-6′), 7.05 (1H, d, *Jortho* = 7.00 Hz, H-3), 7.53 (1H, dd, *Jortho* = 9.1 Hz and *Jmeta* = 1.1 Hz, H-6), 7.82 (1H, d, *Jortho* = 1.1 Hz, H-8), 8.00 (1H, d, *Jortho* = 9.1 Hz, H-5), 8.39 (1H, d, *Jortho* = 7.00 Hz, H-2); ^{13}C NMR (D_2O, 100 MHz) (Fig. S13): $\delta = 41.5$ ($\underline{C}H_2$), 45.8 ($\underline{C}H_2$), 50.1 ($\underline{C}H_2$), 51.0 ($\underline{C}H_2$), 55.7 (CH_3, ArO$\underline{C}H_3$), 56.1 (CH_3, ArO$\underline{C}H_3$), 56.2 (CH_3, ArO$\underline{C}H_3$), 97.6 (CH, C-3′), 105.2 (CH, C-6′), 111.1 (CH, C-3), 114.0 (C, C-1′), 117.5 (C, C-4a), 119.1 (C, C-6), 126.8 (CH, C-5), 127.8 (CH, C-8), 139.2 (C, C-2′), 139.5 (C, C-7), 141.3 (CH, C-2), 142.2 (C, C-5′), 150.0 (C, C-4′), 150.6 (C, C-8a), 161.1 (C, C-4), 169.8 (C, $\underline{C}$=O); HRESIMS *m/z* (Fig. S14): $[M+H]^+$ 442.15255 $C_{23}H_{25}ClN_3O_4$ (calcd. 442.15281).

Synthesis of the designed 4-amino-quinazoline analogs 9a and 9b

In a 50 mL flask equipped with a reflux condenser, the 4-chloroquinazoline **12** (180 mg, 1.09 mmol) was dissolved in 20 mL of isopropyl alcohol. Next, 1.1 equivalents of the corresponding benzamide intermediate (**13a** or **13b**) and 5 drops of triethylamine (Et_3N) were added. The resulting reaction mixture was stirred and heated at 82 °C until completion of the reaction, verified by TLC (10% methanol: 90% dichloromethane). The reaction medium was concentrated under reduced pressure and redissolved in ethyl acetate. The resulting products were isolated and purified by extraction in a separation funnel. The organic layer was then dried over anhydrous sodium sulfate, filtered and concentrated under reduced pressure (Scheme 1b).

2,4,5-trimethoxy-*N*-(2-(quinazolin-4-ylamino)ethyl)benzamide (9a) This compound was obtained from the benzamide intermediate **13a** and isolated after liquid–liquid extraction employing an aqueous phase pH around 6 as a pure white powder; yield: 72%; ^{1}H NMR (DMSO-d_6, 400 MHz) (Fig. S15): $\delta = 3.61$ (2H, t, $J = 5.50$ Hz, ArHNC$\underline{H}_2$), 3.74 (5H, m, CONHC$\underline{H}_2$ and ArOC$\underline{H}_3$), 3.78 (3H, s, ArOC$\underline{H}_3$), 3.83 (3H, s, ArOC$\underline{H}_3$), 6.71 (1H, s, H-3′), 7.43 (1H, s, H-6′), 7.52 (1H, t, *Jortho1* = 7.5 Hz and *Jortho2* = 8.10 Hz, H-6), 7.68 (1H, d, *Jortho* = 8.10 Hz, H-5), 7.76 (1H, t, *Jortho1* = 7.50 Hz and *Jortho2* = 8.0 Hz, H-7), 8.23 (1H, t, *Jortho* = 8.0 Hz, H-8), 8.30 (1H, t, $J = 5.50$ Hz, NHAr), 8.42 (1H, t, $J = 5.20$ Hz, CONH), 8.47 (1H, s, H2); ^{13}C NMR (DMSO-d_6, 100 MHz) (Fig. S16): $\delta = 38.7$ ($\underline{C}H_2$), 40.3 ($\underline{C}H_2$), 55.9 (CH_3, ArO$\underline{C}H_3$), 56.5 (CH_3, ArO$\underline{C}H_3$), 97.7 (CH, C-3′), 112.8 (C, C-1′), 113.6 (CH, C-6′), 115.0 (C, C-8a), 122.6 (CH, C-6), 125.7 (CH, C-8), 127.5 (CH, C-5), 132.6 (CH, C-7), 142.4 (C, C-4a), 149.1 (C, C-2′), 152.1 (C, C-5′), 152.5 (C, C-4′), 155.1 (CH, C-2), 159.6 (C, C-4), 164.7 (C, $\underline{C}$=O); HRESIMS *m/z* (Fig. S17): $[M+H]^+$ 383.17094 $C_{20}H_{23}N_4O_4$ (calcd. 383.17138).

(4-(quinazolin-4-yl)piperazin-1-yl)(2,4,5-trimethoxyphenyl) methanone (9b) Compound **9b** was obtained from the benzamide intermediate **13b** and isolated after a liquid–liquid extraction employing an aqueous phase pH around 9, followed by an additional purification acid-base extraction for removing an undesired side product. For that, product **9b** was extracted from the organic layer with an aqueous solution of HCl (pH = 3). Afterwards, pH of the aqueous layer was adjusted to neutrality and the pure derivative **9b** was extracted back to the organic layer. The final organic layers containing **9b** were then dried over anhydrous sodium sulfate, filtered and concentrated under reduced pressure, giving **9b** as a pure beige powder; yield: 54%; ^{1}H NMR (acetone-d_6, 400 MHz) (Fig. S18): $\delta = 3.58$ (4H, br, C$\underline{H}_2$), 3.82 (3H, s, ArOC$\underline{H}_3$), 3.90 (3H, s, ArOC$\underline{H}_3$), 3.92 (3H, s, ArOC$\underline{H}_3$), 3.98 (4HH, br, C$\underline{H}_2$), 6.81 (1H, s, H-3′), 6.91 (1H, s, H-6′), 7.57 (1H, t, *Jortho* = 7.5 Hz, H-6), 7.87 (2H, m, H-5 and H-7), 8.13 (1H, d, *Jortho* = 8.3 Hz, H-8), 8.71 (1H, s, H-2); ^{13}C NMR (acetone-d_6, 100 MHz) (Fig. S19): $\delta = 42.1$ (CH_2, ArN$\underline{C}H_2$), 47.3 (CH_2, ArN$\underline{C}H_2$), 50.4 (CH_2, CON$\underline{C}H_2$), 50.9 (CH_2, CON$\underline{C}H_2$), 56.3 (CH_3, ArO$\underline{C}H_3$), 56.7 (CH_3, ArO$\underline{C}H_3$), 56.9 (CH_3, ArO$\underline{C}H_3$), 98.6 (CH, C-3′), 113.7 (CH, C-6′), 117.5 (C, C-1′), 117.8 (C, C-4a), 126.1 (CH, C-6), 126.5 (CH, C-8), 129.4 (CH, C-5), 133.4 (CH, C-7), 144.4 (C, C-2′), 151.0 (C, C-5′), 152.0 (C, C-4′), 152.9 (C, C-8a), 154.7 (CH, C-2), 165.4 (C, C-4), 167.6 (C, $\underline{C}$=O); HRESIMS *m/z* (Fig. S20): $[M+H]^+$ 409.18656 $C_{22}H_{25}N_4O_4$ (calcd. 409.18703).

Molecular docking

Initially, the three-dimensional structures of the compounds were constructed on Avogadro software (version 1.2.0) (Hanwell et al. 2012), and their energy was minimized using Merck molecular force field (MMFF94) (Halgren 1996). We then performed the blind docking between the compounds and mouse PrP globular domain (PDB: 1AG2) using AutoDock software (version 4.2.6) (Morris et al. 2009). The protein was set rigid, and the ligands were set flexible. The search space was centered on *x*-, *y*- and *z*-coordinates of −3.000, 0.752, and −1.572, respectively, and defined in a grid of 126 × 126 × 126 points with default 0.375 Å spacing. We considered the neutral ε-tautomeric state for His177 and His187 and the neutral δ-tautomeric state for His140, according to previous work (Langella et al. 2006; Malevanets et al. 2017). A total of 50 docking runs were performed using the Lamarckian Genetic Algorithm (LGA) and default parameters. In the next step, we performed a site-directed molecular docking based on a

previously described method (Ferreira et al. 2018). The search space was centered on *x*-, *y*- and *z*-coordinates of 4.913, 7.305, and 2.540, respectively, and defined in a grid of 64 × 58 × 54 points. LGA parameters were the same used in the blind docking. The selected conformer was the one that presented the lowest Gibbs free energy (ΔG) of binding. GN8 (**4**) was used to validate the site-directed molecular docking.

Real-time quaking induced conversion (RT-QuIC)

The RT-QuIC assay was performed as previously described (Wilham et al. 2010). The brain homogenate was diluted in PBS containing 0.1% SDS and N2 medium supplement (GIBCO) (SDS–PBS–N2). We loaded each well of a black-walled, clear-bottom 96-well plate (Nunc) with 90 µL of the reaction medium, which had the following composition: 10 mM phosphate buffer (pH 7.4); 170 mM NaCl; 10 µM EDTA; 10 µM ThT; and hamster $rPrP^{90–231}$ at 0.1 mg/mL (6 µM) or hamster $rPrP^{23–231}$ at 0.1 mg/mL (4.3 µM). Then, we added 2 µL of brain homogenate (1×10^5 dilution) and 8 µL of stock solutions of the compounds to reach the final concentrations of 40, 50, 100, and 200 µM. The plates were sealed with a plate sealer film (Nalgene Nunc International) and incubated on a BMG FLUOstar plate reader (BMG Biotech), at 42 °C, under continuous cycles of 1 min of double-orbital shaking at 700 rpm and 1 min of rest. ThT fluorescence readings were performed every 15 min (excitation at 450 ± 10 nm and emission at 480 ± 10 nm). Post-mortem-collected sporadic Creutzfeldt-Jakob disease (sCJD) brain tissue was obtained from Prof. Pierluigi Gambetti at Case Western Reserve University and was used under Exemption #11197 from the NIH Office of Human Subjects Research Protections.

Saturation transfer difference nuclear magnetic resonance (STD-NMR)

NMR spectra were collected at 25 °C on a 600 MHz Bruker Avance III spectrometer equipped with a room temperature inverse-detection 5-mm TXI probe. The mixture contained **8a** or **8b** at 1 mM and murine $rPrP^{90–231}$ at 10 µM in 100% D_2O (1:100 protein:ligand molar ratio). Protein signals were selectively saturated using 60 Gaussian-shaped pulses of 50 ms each, resulting in a total saturation time of 3 s. A relaxation delay of 3 s was used during the STD-NMR experiment, taking into consideration the long T1 values of the ligands. Selective protein saturation occurred at different frequencies. On-resonance saturation occurred at –0.19, 0.12, 0.76, 6.52, 6.62 ppm for **8b**–rPrP interaction and at –0.11, 0.21, 0.38, 7.28, 8.45 ppm for **8a**–rPrP interaction, while off-resonance saturation occurred at –10 ppm. STD-NMR experiments were acquired with 48 scans and Watergate sequence was used for residual water suppression. A 40 ms spinlock filter was applied to suppress protein background signals. A 3 Hz line broadening was applied to FID prior to Fourier transformation. STD-NMR spectra were obtained by subtracting the on- from the off-resonance spectra.

Isothermal titration calorimetry (ITC)

Binding studies between $rPrP^{90–231}$ and the compounds were performed at 25 °C on an ITC-200 microcalorimeter (Malvern MicroCal, USA). Both protein and ligand working solutions were prepared in 10 mM phosphate buffer (pH 7.4) containing 150 mM NaCl. The syringe was filled with compound working solutions, while 200 µL of rPrP working solution was placed into the sample cell. The reference cell was loaded with degassed ultrapure water. Then, we performed a single injection of 20 µL at an interval of 180 s, during which the solution was stirred at 750 rpm with the syringe inside the sample cell with no foaming. For **8a** analysis, the **8a** solution in the syringe was at 1 mM and the rPrP solution in the sample cell was at 10 µM. For **8b** analysis, the **8b** solution in the syringe was at 0.5 mM and the rPrP solution in the sample cell was at 5 µM. In both cases, the protein:ligand molar ratio was 1:10. The heat of dilution of the compounds in buffer was subtracted from the heat of dilution of the compounds in rPrP solution. Analysis of ITC data was carried out on Origin 7.0.

Dot blot

The dot blot assay was performed as previously described (Ferreira et al. 2018) with ScN2a cells infected with prion strains RML or 22 L. Each treatment was tested in quadruplicate. The vehicle for the compounds at 0.1, 0.5, 1, and 10 µM corresponded to PBS (pH 7.4) containing DMSO at 0.001%, 0.005%, 0.01%, and 0.1%, respectively. We used the primary antibody 6D11 (1:7,500; sc-58581) and the alkaline phosphatase-conjugated secondary antibody.

MTT reduction

Cell viability in the presence of the compounds was followed by the MTT reduction assay as previously described (Ferreira et al. 2014) using ScN2a cells infected with prion strains RML or 22 L. Each treatment was tested in quadruplicate. The vehicle for the compounds at 0.1, 0.5, 1, and 10 µM corresponded to PBS (pH 7.4) containing DMSO at 0.001%, 0.005%, 0.01%, and 0.1%, respectively.

Statistical analysis

Data from dot blot and MTT reduction assays were analyzed using one-way ANOVA with Dunnett's multiple

comparisons test. All statistical evaluations were performed with GraphPad Prism 8 software.

Results and discussion

Structural design

Starting from the anti-prion prototypes 4-amino-quinoline **5** (Macedo et al. 2010) and trimethoxy-chalcone **6** (Ferreira et al. 2014), the first heterocyclic trimethoxy-benzamide analog **8a** was designed by molecular hybridization, linking the structural fragments **A** and **B** from compound **5** to the fragment **C** from compound **6** in the novel hybrid structure of **8a**, as depicted in Fig. 2. Aiming to evaluate the possible influence of conformational flexibility on the ability to interact with the target, i.e., the prion protein, the conformationally restricted analog **8b** was also planned. Moreover, to assess the relevance of 7-chloro-4-amino-quinoline heterocyclic moiety **A** for the anti-prion activity of this novel hybrid compounds, derivatives **9a** and **9b**, bearing a 4-amino-quinazoline **A'** core, were designed. The heterocyclic nucleus **A'** was selected due to its well-known property of acting as a privileged scaffold in Medicinal Chemistry, since the 4-amino-quinazoline nucleus has been extensively studied for its wide range of pharmacological and therapeutic effects (Kamal et al. 2006; Waiker et al. 2014; Khan et al. 2015).

In turn, the bis-trimethoxy-benzamide analog **10a** was designed by molecular hybridization, combining the fragment **C** from trimethoxy-chalcone **6** (Ferreira et al. 2014) with the ethylenediamine **B** from 4-amino-quinoline prototype **5** (Macedo et al. 2010), furnishing the hybrid derivative **10a**, which encloses two trimethoxy-phenyl rings separated by a spacer, in a direct analogy to the structure of the anti-prion prototype **6** (Fig. 2). Once again, the influence of the conformational flexibility was considered for the design of the conformationally restricted piperazine analog **10b**.

Chemical synthesis

The target heterocyclic trimethoxy-benzamide derivatives **8a**, **8b**, **9a**, and **9b** were synthesized via nucleophilic aromatic substitution (S_NAr) by a key condensation step between the 4-chloro-heterocycles (**11** or **12**) and the corresponding amidic intermediates (**13a** or **13b**) (Sashidhara et al. 2012; Kershaw et al. 2013; Braga et al. 2017), as depicted in Scheme 1. 7-chloro-4-amino-quinoline derivatives **8a** and **8b** precipitated directly from the reaction media, which was favorable for shifting the reaction balance to their formation. In the case of the synthesis of 4-amino-quinazolines **9a** and **9b**, no precipitation was observed and the addition of triethylamine (Et_3N) was necessary to absorb the hydrochloric acid by-product, favoring product formation.

All heterocyclic trimethoxy-benzamide derivatives **8a**, **8b**, **9a**, and **9b** were characterized by ^{1}H and ^{13}C NMR and HRMS and showed spectral data consistent with the assigned structures. As expected, the mass spectra of the 7-chloro-4-amino-quinoline products **8a** and **8b** revealed the isotopic clusters predicted for monochlorinated molecules. The HRMS spectra of **8a** and **8b** displayed ions with a 3:1 relative abundance, which is the *m/z* expected for the ^{35}Cl and ^{37}Cl isotopic ratio (Trivedi et al. 2016).

For the synthesis of trimethoxy-benzamide intermediates **13a** and **13b**, as well as for obtaining the target bis-trimethoxy-benzamide analogs **10a** and **10b**, the acyl-chloride **14** was employed as starting material (Ahmad et al. 2010; Mallikarjuna et al. 2016) (Scheme 2). The favored formation of the monoamides **13a** and **13b** or the bis-amides **10a** and **10b** was easily managed with the proper adjustments in the synthetic methodology in terms of number of amine equivalents and order of addition of the reagents. In other words, for the synthesis of trimethoxy-benzamide intermediates **13a** and **13b**, a solution of the acyl-chloride **14** in dichloromethane was slowly added dropwise into a dichloromethane solution containing a great excess of ethylenediamine or piperazine (10 eq). In turn, for

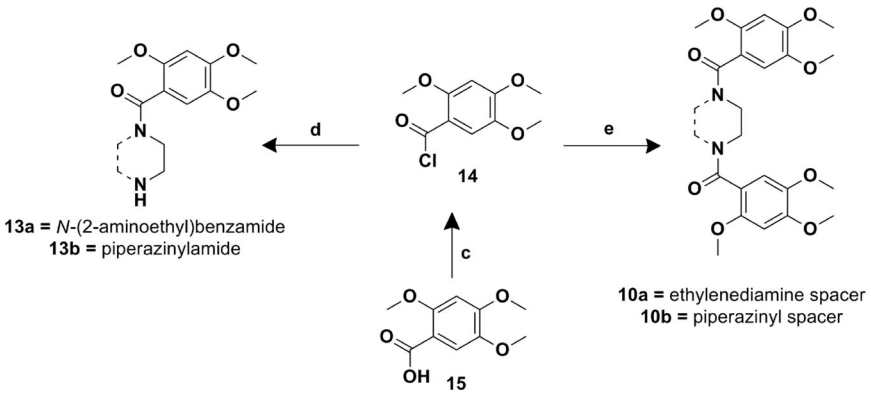

Scheme 2 Reagents and conditions: **c** oxalyl chloride, CH_2Cl_2, cat. DMF, r.t., 2 h, 100%; **d** A solution of the acyl-chloride **14** in CH_2Cl_2 was slowly added dropwise into a piperazine or ethylenediamine 10eq solution, CH_2Cl_2, r.t., 20', 75–95%; **e** piperazine or ethylenediamine (1–4 eq) were slowly added into a CH_2Cl_2 solution of **14** until its complete consumption was observed, r.t., 2 h, 82–87%

the synthesis of the designed bis-trimethoxy-benzamides **10a** and **10b**, the corresponding amines, i.e., ethylenediamine or piperazine, were slowly added to a solution of the acyl-chloride **14** in dichloromethane until the complete consumption of **14** was observed. In the described conditions, only trace amounts of the undesired products were detected by TLC monitoring. The acyl-chloride **14** was obtained from the corresponding benzoic acid **15** by classical functional group interconversion (Ahmad et al. 2010), as detailed in Scheme 2.

All benzamide derivatives **10a**, **10b**, **13a**, and **13b** were characterized by ^{1}H and ^{13}C NMR. Moreover, the designed bis-trimethoxy-benzamide analogs **10a** and **10b** were analyzed by HRMS and showed spectral data consistent with the assigned structures.

Interaction between PrP and trimethoxy-benzamide derivatives assessed by molecular docking

In order to investigate the binding mode of the trimethoxy-benzamide derivatives, we docked them into mouse PrP globular domain (PDB: 1AG2) using AutoDock software. Initially, we performed a blind docking, which reinforced that their most probable site of interaction within PrP globular domain was the *hotspot* region, previously described (Langella et al. 2004; Kuwata et al. 2007). In order to further explore the specific interaction of these compounds with the PrP *hotspot* site, we firstly docked GN8 (**4**) into this pocket and obtained interactions and spatial orientation in accordance with the results found by Kuwata's group (Kuwata et al. 2007; Yamamoto and Kuwata 2009; Ishikawa et al. 2009) (Fig. S21). The validated docking methodology was then performed with the trimethoxy-benzamide analogs. All these compounds exhibited similar orientation and hydrogen bonding with Lys194 (ranging from 2.6 to 3.3 Å) and Asn159 (ranging from 2.6 to 3.5 Å), as well as hydrophobic interactions with Leu125, Leu130, Gln160, Val161, Tyr162, Ile182, Thr183, and Gln186 (Figs. 3 and S22). Their binding energy to PrP ranged from –6.35 to –7.88 kcal/mol, which was similar to the value found for GN8 binding (–8.83 kcal/mol) (Figs. 3 and S21). In summary, these results suggested that these molecules might act as PrP ligands.

Modulation of rPrP aggregation assessed by RT-QuIC

The real-time quaking induced conversion (RT-QuIC) is a cell-free diagnostic tool widely used to detect and amplify minute amounts of PrP^{Sc} from different biological samples, such as brain, cerebrospinal fluid, blood, nasal brushing, saliva, urine, and feces (Wilham et al. 2010; Atarashi et al. 2011; Orru et al. 2017). In this assay, soluble, monomeric rPrP is used as substrate, and the infectious particles in the biological samples seed the conversion of monomeric rPrP into rPrP fibrils under specific shaking and temperature conditions. The conversion is monitored in real-time by thioflavin T (ThT), an amyloidophilic dye which binds to newly formed rPrP fibrils (Wilham et al. 2010). Besides its usefulness for diagnostic purposes, this assay has been employed in the last years to identify inhibitors of rPrP aggregation in vitro (Ferreira et al. 2014, 2018; Vieira et al. 2014; Schmitz et al. 2016; Hyeon et al. 2017).

As all trimethoxy-benzamide derivatives were predicted to bind to PrP globular domain, we investigated whether they could inhibit rPrP conversion in the RT-QuIC assay. We performed the reactions using hamster $rPrP^{90–231}$ as substrate and brain homogenate from a patient with sCJD as a source of PrP^{Sc}. At all concentrations tested (50, 100, and 200 μM), the analogs neither inhibited the conversion nor delayed the process, except for **8a**, which shortened the lag phase (Figs. 4 and S23). These findings indicate that the putative interaction of the designed compounds with PrP^{C}, as predicted by molecular docking, was not able to prevent monomeric rPrP conversion into rPrP aggregates in vitro. However, the reduced lag phase observed in the presence of **8a** suggests that this derivative might interact with PrP globular domain.

In order to exclude the possibility that the compounds could be quenching ThT fluorescence rather than inhibiting rPrP fibrillation, the analogs were added to the RT-QuIC reaction media after the conversion reached the plateau (17 h). No decrease in ThT fluorescence was observed (Fig. S24).

Although no inhibitory effect in the prion conversion assay was observed, it is relevant to highlight that we were able to identify a new chemical entity (NCE) bearing a novel 4-amino-quinoline trimethoxy-benzamide structural pattern, i.e., **8a**, which was able to modulate rPrP aggregation in vitro. Based on these data, the 4-amino-quinoline heterocyclic moiety was considered as preferential for the proposed interaction with PrP^{C}; thus **8a** represents a useful starting point for future structural optimization in the design of novel anti-prion drug candidates.

Interaction between rPrP and trimethoxy-benzamide derivatives assessed by STD-NMR and ITC

Considering the results from the RT-QuIC assay, we next performed a saturation transfer difference nuclear magnetic resonance (STD-NMR) experiment to investigate the direct interaction of compound **8a** and its conformationally restricted analog **8b** with mouse $rPrP^{90–231}$.

STD-NMR signals were observed for nearly all hydrogens of **8a** (hydrogens 2 and/or 5, 6, 8, 3′, 6′, and methoxyl

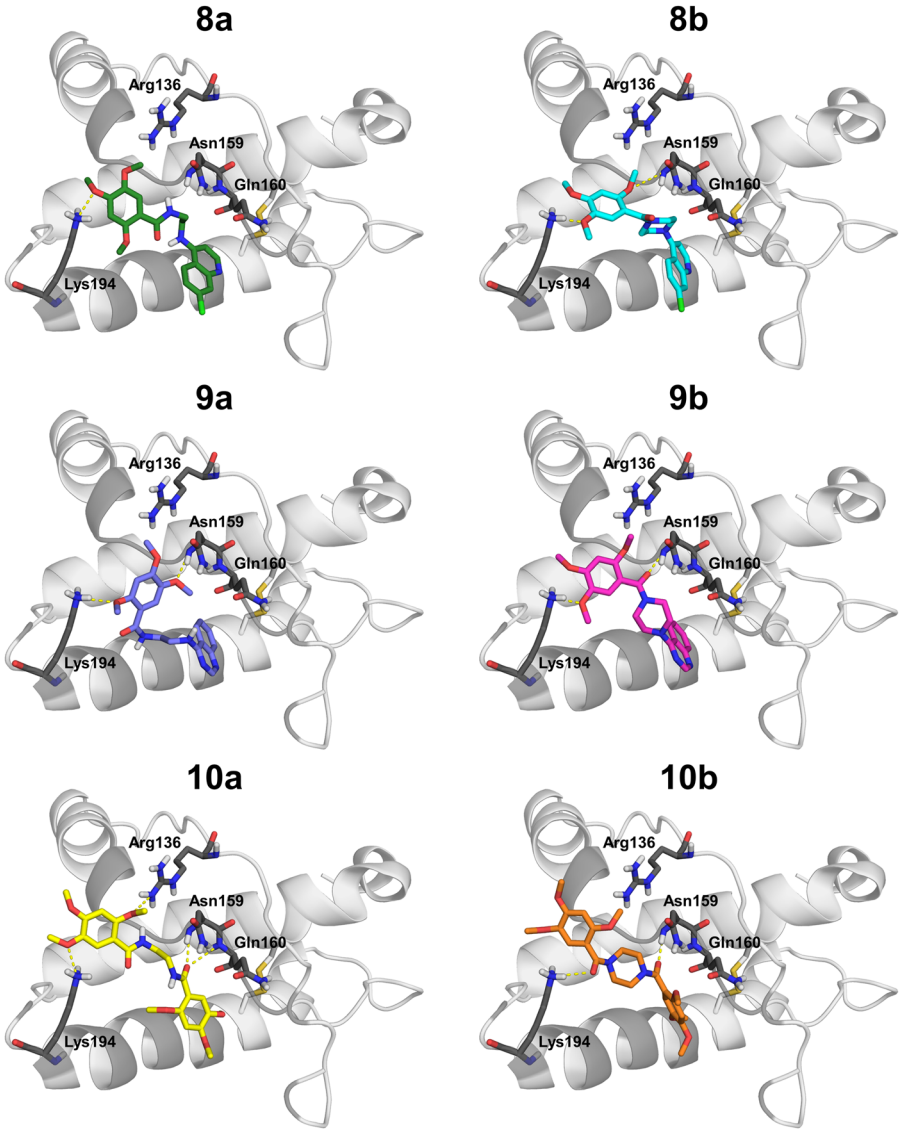

Fig. 3 Binding mode analysis of the trimethoxy-benzamide analogs with mouse PrP globular domain (PDB: 1AG2). Residues involved on the interactions are highlighted in dark gray, and hydrogen bonds are colored in yellow dashed lines. The binding energy values were the following: –7.00 kcal/mol for **8a**, –7.66 kcal/mol for **8b**, –6.78 kcal/mol for **9a**, –7.88 kcal/mol for **9b**, –6.35 kcal/mol for **10a**, and –6.90 kcal/mol for **10b**

groups) and **8b** (hydrogens 2, 3, 5, 8, 3′, 6′, and methoxyl groups) in the presence of $rPrP^{90–231}$, suggesting that both ligands bind directly to $rPrP^{90–231}$ via hydrophobic interactions (Fig. 5). The signals highlighted at approximately 6.6 ppm (Fig. 5c), 7.3 ppm, and 8.5 ppm (Fig. 5b) correspond to protein resonances that were selectively saturated, despite the spinlock filter used during the experiment.

Comparison of the STD-NMR spectra obtained for **8a** and **8b** in complex with $rPrP^{90–231}$ suggests that the binding epitope for both ligands are similar, reinforcing the relevance of the 4-amino-quinoline and trimethoxy-benzamide moieties for this complementary molecular recognition. Interestingly, **8b** showed higher intensity STD-NMR signals than **8a**, suggesting that **8b** has a tighter interaction with $rPrP^{90–231}$. In contrast, **8b** yielded no significant change in the RT-QuIC assay.

We also analyzed the interaction of **8a** and **8b** with $rPrP^{90–231}$ using single-injection isothermal titration calorimetry (ITC). Addition of either **8a** or **8b** to $rPrP^{90–231}$ produced an endothermic heat of reaction (Fig. 6), which indicated that both compounds display mainly hydrophobic interactions with $rPrP^{90–231}$. This is in accordance with the results from the STD-NMR analysis.

Cellular efficacy/toxicity evaluation of trimethoxy-benzamide derivatives

We next investigated whether the analogs **8a** and **8b** could change PrP^{Res} levels in PrP^{Sc}-infected murine neuroblastoma (ScN2a) cells. This method has been extensively used to assess the anti-prion activity of molecules, as it employs a robust and relatively economical model and

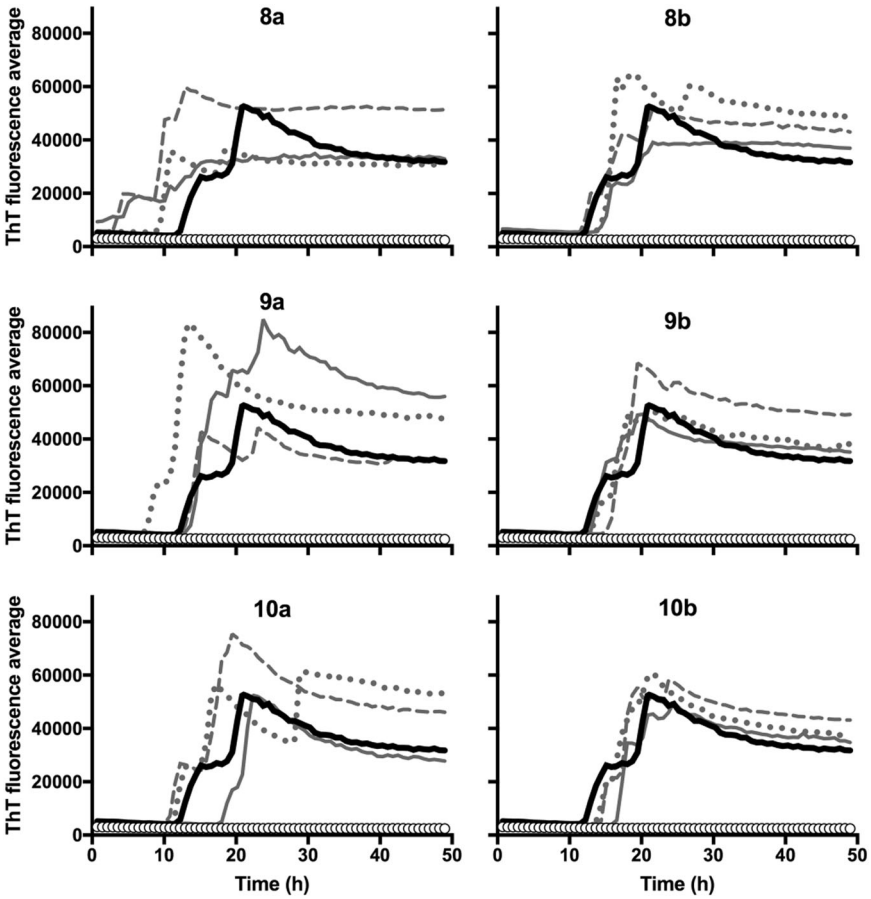

Fig. 4 RT-QuIC kinetics using hamster $rPrP^{90–231}$ at 6 μM as the substrate and sCJD agent-infected human brain homogenate as the seed. The reactions were performed in the absence (solid black line) or in the presence of the compounds at 50 μM (dotted gray line), 100 μM (dashed gray line), and 200 μM (solid gray line). Normal brain homogenate (NBH) was used as a negative control of seeding (white circles). Each curve represents the average ThT fluorescence of four replicates. The individual replicates are plotted in Fig. S23

allows the evaluation of prion strain-related effects (Kocisko et al. 2003). We treated both RML-strain ScN2a (ScN2a-RML) and 22L-strain ScN2a (ScN2a-22L) cell lines with **8a** and **8b** at concentrations ranging from 0.1 to 10 μM. In ScN2a-RML cells, **8b** induced a significant decrease in PrP^{Res} content at 1 and 10 μM, while **8a** promoted a similar outcome only at 10 μM (Fig. 7). In ScN2a-22L cells, both **8a** and **8b** prompted a significant decrease in PrP^{Res} content only at 10 μM (Fig. 7).

Simultaneously, we examined whether the compounds were affecting cell viability. Both **8a** and **8b** significantly reduced ScN2a-RML and ScN2a-22L cell viability at 10 μM, while **8b** also significantly decreased ScN2a-RML cell viability at 1 μM (Fig. 7). The PrP^{Res} content reduction profiles were reasonably correlated with the cell viability reduction profiles (Fig. 7). These results indicated that these compounds were decreasing the final PrP^{Res} levels by inducing cell death rather than by effectively inhibiting PrP^{Res} formation and/or promoting PrP^{Res} clearance.

The analogs **9a** and **9b** exhibited similar profiles to those displayed by **8a** and **8b**, while **10b** was neither effective in decreasing PrP^{Res} content nor significantly cytotoxic (Fig. S25). The derivative **10a** was also non-toxic and promoted moderate reduction in PrP^{Res} levels at the concentration of 10 μM (Fig. S25). These results suggested that the 7-chloro-4-amino-quinoline and 4-amino-quinazoline portions are toxicophoric in the cell lines used, while the trimethoxy-benzamide region is not.

Although the analogs **8a**, **8b**, **9a**, and **9b** were toxic to ScN2a cells, they were not equally toxic to other mammalian cell lines, including human cell lines (data not shown). These findings indicated that the 7-chloro-4-amino-quinoline and 4-amino-quinazoline rings are not universally toxicophoric, thus these compounds might even be tested in other PrP^{Sc}-infected cell lines.

Conclusion

This study has described the synthesis and biological testing of a novel series of trimethoxy-benzamide derivatives (**8a**, **8b**, **9a**, **9b**, **10a**, and **10b**) designed as anti-prion compounds. Molecular docking studies predicted that all the compounds were expected to bind to a *hotspot* region in PrP globular domain with very similar spatial orientation and interaction mode. The analogs were then further evaluated by RT-QuIC and, although none of them prevented the conversion of monomeric $rPrP^{90–231}$ into rPrP fibrils, the

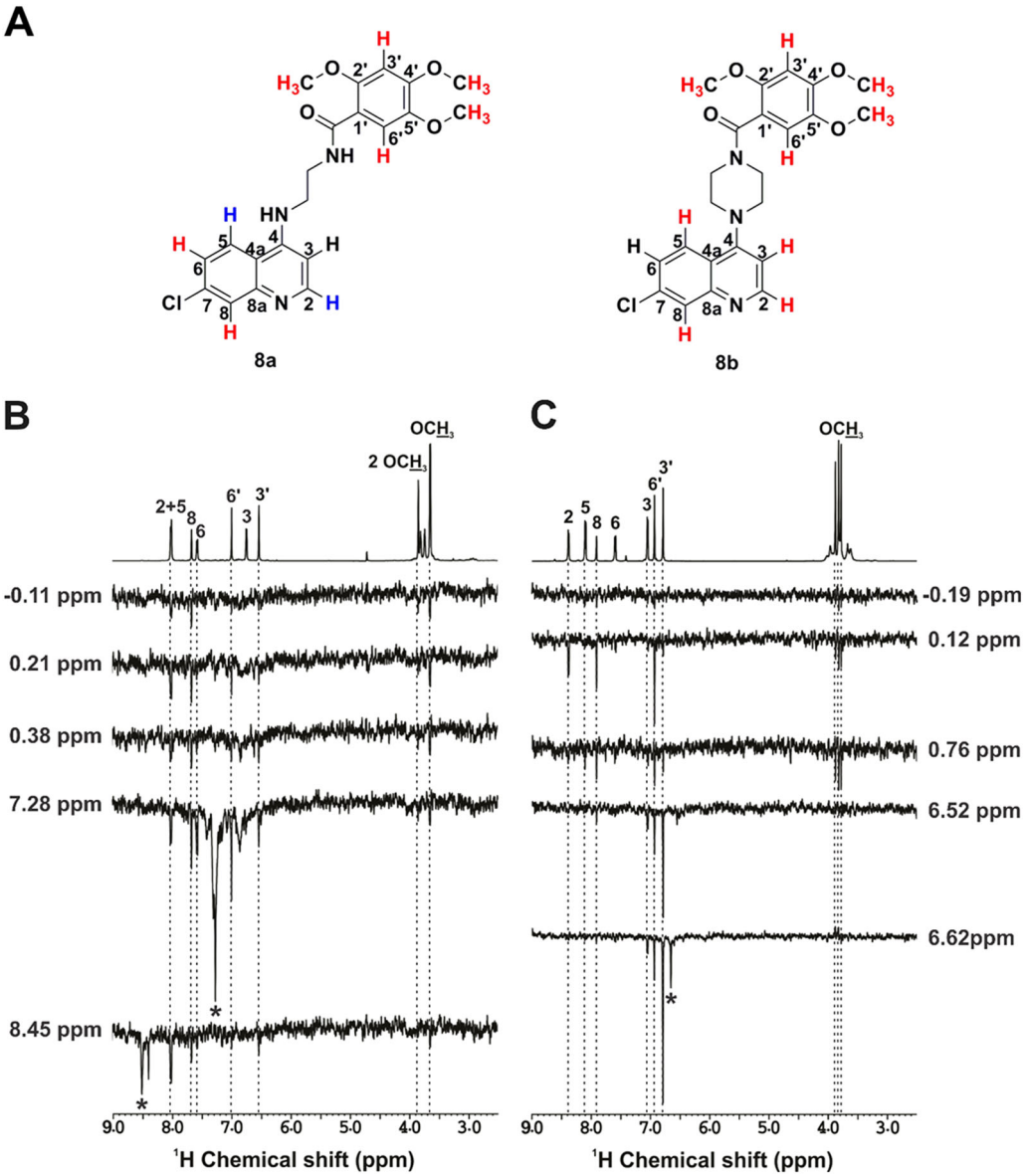

Fig. 5 STD-NMR spectra of **8a** and **8b** in complex with mouse $rPrP^{90–231}$. **a** Chemical structures of **8a** and **8b**, with the corresponding hydrogens showing STD-NMR signals highlighted in red. For **8a**, hydrogens 2 and 5 are highlighted in blue, since they could not be discriminated by their STD-NMR signals. **b** STD-NMR spectra of 1 mM **8a** in the presence of 10 µM rPrP in 100% D_2O. ^1H off-resonance, reference spectrum is depicted on top of the figure. Each STD-NMR spectrum was collected in a different on-resonance frequency: –0.11, 0.21, 0.38, 7.28, 8.45 ppm, as indicated. **c** STD-NMR spectra of 1 mM **8b** in the presence of 10 µM rPrP in 100% D_2O. ^1H reference spectrum is depicted on top of the figure. Each STD-NMR spectrum was collected in a different on-resonance frequency: –0.19, 0.12, 0.76, 6.52, 6.62 ppm, as indicated

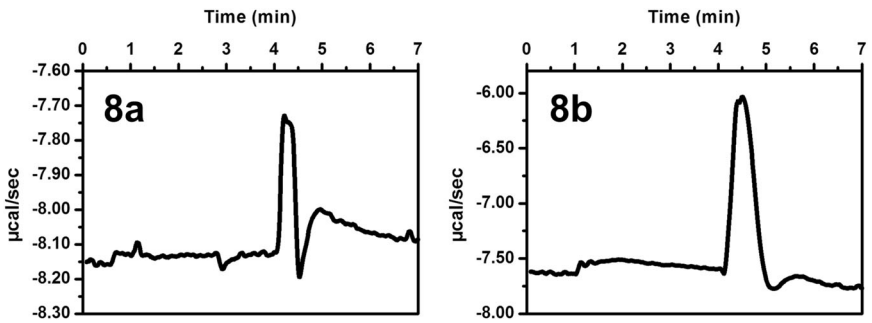

Fig. 6 Single-injection ITC binding isotherm of **8a** and **8b** to mouse $rPrP^{90–231}$. The curves shown were normalized by subtracting the heat of dilution of the compounds in buffer from the heat of dilution of the compounds in rPrP solution. The experiment was carried out at 25 °C with protein:ligand molar ratio of 1:10

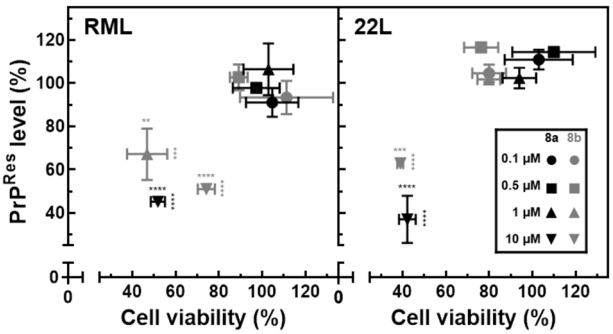

Fig. 7 Effect of **8a** and **8b** on PrP^{Res} content and cell viability in PrP^{Sc}-infected murine neuroblastoma (ScN2a) cells. ScN2a cells infected with RML strain (left) or 22L-strain (right) were treated with **8a** (black) or **8b** (gray) at the concentrations of 0.1 µM (•), 0.5 µM (■), 1 µM (▲), and 10 µM (▼). The vehicle for the compounds at 0.1, 0.5, 1, and 10 µM corresponded to PBS (pH 7.4) containing DMSO at 0.001%, 0.005%, 0.01%, and 0.1%, respectively. The PrP^{Res} content was determined by dot blot assay using anti-PrP antibody 6D11. Cell viability was determined by MTT reduction assay

analog **8a** shortened the lag phase for conversion, suggesting interaction with rPrP. As partial denaturation is supposed to precede PrP aggregation into PrP^{Sc}-like species (Kocisko et al. 1994), we speculate whether **8a** can promote unfolding of PrP^{C}, thus accelerating fibrillation. However, additional experiments are necessary to sustain this hypothesis. STD-NMR and ITC analyses indicated that the derivative **8a** and its conformationally restricted analog **8b** bind to $rPrP^{90–231}$ and do so via hydrophobic interactions. These results point the novel 4-amino-quinoline trimethoxybenzamide structure as an original chemical pattern for PrP complementary recognition, although affinity improvement should be aimed in a further structural optimization step. Insertion of additional polar interaction sites with the *hot-spot* region might represent an attractive approach to overcome this issue. The accurate evaluation of the antiprion activity of **8a** and **8b** in cell models was hindered by their toxicity to the PrP^{Sc}-infected cell lines used herein. Notwithstanding, this toxicity was cell line dependent. Derivatives **8a** and **8b** thus represent Novel Chemical Entities useful as starting points for future structural modifications in the design of novel anti-prion drug candidates with optimized efficacy and safety profiles.

Acknowledgements The authors thank the Faculty of Pharmacy of the Federal University of Rio de Janeiro (FF-UFRJ, BR); the Laboratory for the Support of Technological Development of the Federal University of Rio de Janeiro (LADETEC-UFRJ, BR); the Laboratory of Evaluation and Synthesis of Bioactive Substances of the Federal University of Rio de Janeiro (LASSBio-UFRJ, BR); the Laboratory of Persistent Viral Diseases from Rocky Mountain Laboratories of the National Institutes of Health (USA); and the funding agencies INCT-INOFAR (BR), CAPES (BR), CNPq (BR) and FAPERJ (BR) for fellowship and financial support. The authors thank the LAMAR laboratory, from Walter Mors Institute of Research on Natural Products, Federal University of Rio de Janeiro (IPPN-UFRJ, BR) for NMR analysis. This study was financed in part by the *Coordenação de Aperfeiçoamento de Pessoal de Nível Superior* - Brazil (CAPES) - Finance Code 001.

Compliance with ethical standards

Conflict of interest The authors declare that they have no conflict of interest.

Publisher's note Springer Nature remains neutral with regard to jurisdictional claims in published maps and institutional affiliations.

References

Abid K, Morales R, Soto C (2010) Cellular factors implicated in prion replication. FEBS Lett 584:2409–2414. https://doi.org/10.1016/j.febslet.2010.04.040

Ahmad S, Ngu K, Miller KJ et al. (2010) Tricyclic dihydroquinazolinones as novel 5-HT2Cselective and orally efficacious anti-obesity agents. Bioorg Med Chem Lett 20:1128–1133. https://doi.org/10.1016/j.bmcl.2009.12.014

Atarashi R, Satoh K, Sano K et al. (2011) Ultrasensitive human prion detection in cerebrospinal fluid by real-time quaking-induced conversion. Nat Med 17:175–178. https://doi.org/10.1038/nm.2294

Braga SFP, Martins LC, da Silva EB et al. (2017) Synthesis and biological evaluation of potential inhibitors of the cysteine proteases cruzain and rhodesain designed by molecular simplification. Bioorg Med Chem 25:1889–1900. https://doi.org/10.1016/j.bmc.2017.02.009

Castle AR, Gill AC (2017) Physiological functions of the cellular prion protein. Front Mol Biosci 4:19. https://doi.org/10.3389/fmolb.2017.00019

Caughey B, Baron GS, Chesebro B, Jeffrey M (2009) Getting a grip on prions: oligomers, amyloids, and pathological membrane interactions. Annu Rev Biochem 78:177–204. https://doi.org/10.1146/annurev.biochem.78.082907.145410

Cordeiro Y, Ferreira NC (2015) New approaches for the selection and evaluation of anti-prion organic compounds. Mini Rev Med Chem 15:84–92. https://doi.org/10.2174/1389575156661502271116 29

Ferreira NC, Ascari LM, Hughson AG et al. (2018) A promising antiprion trimethoxychalcone binds to the globular domain of the cellular prion protein and changes its cellular location. Antimicrob Agents Chemother 62:e01441-17. https://doi.org/10.1128/AAC.01441-17

Ferreira NC, Marques IA, Conceição WA et al. (2014) Anti-prion activity of a panel of aromatic chemical compounds: in vitro and in silico approaches. PLoS ONE 9:e84531. https://doi.org/10.1371/journal.pone.0084531

Forloni G, Artuso V, Roiter I et al. (2013) Therapy in prion diseases. Curr Top Med Chem 13:2465–2476. https://doi.org/10.2174/15680266113136660173

Geschwind MD, Kuo AL, Wong KS et al. (2013) Quinacrine treatment trial for sporadic creutzfeldt-Jakob disease. Neurology 81:2015–2023. https://doi.org/10.1212/WNL.0b013e3182a9f3b4

Ghaemmaghami S, Russo M, Renslo AR (2014) Successes and challenges in phenotype-based lead discovery for prion diseases. J Med Chem 57:6919–6929. https://doi.org/10.1021/jm5001425

Haïk S, Marcon G, Mallet A et al. (2014) Doxycycline in Creutzfeldt-Jakob disease: a phase 2, randomised, double-blind, placebo-controlled trial. Lancet Neurol 13:150–158. https://doi.org/10.1016/S1474-4422(13)70307-7

Halgren TA (1996) Merck molecular force field. I. Basis, form, scope, parameterization, and performance of MMFF94. J Comput Chem 17:490–519.

Hanwell MD, Curtis DE, Lonie DC et al. (2012) Avogadro: an advanced semantic chemical editor, visualization, and analysis platform. J Cheminform 4:1–17. https://doi.org/10.1186/1758-2946-4-17

Hyeon JW, Choi J, Kim SY et al. (2015) Discovery of novel anti-prion compounds using in silico and in vitro approaches. Sci Rep 5:14944. https://doi.org/10.1038/srep14944

Hyeon JW, Kim SY, Lee SM et al. (2017) Anti-prion screening for acridine, dextran, and tannic acid using real time–quaking induced conversion: a comparison with PrPSc-infected cell screening. PLoS ONE 12:e0170266. https://doi.org/10.1371/journal.pone.0170266

Ishibashi D, Nakagaki T, Ishikawa T et al. (2016) Structure-based drug discovery for prion disease using a novel binding simulation. EBioMedicine 9:238–249. https://doi.org/10.1016/j.ebiom.2016.06.010

Ishikawa T, Ishikura T, Kuwata K (2009) Theoretical study of the prion protein based on the fragment molecular orbital method. J Comput Chem 30:2594–2601. https://doi.org/10.1002/jcc.21265

Kamal A, Reddy KL, Devaiah V et al. (2006) Recent advances in the solid-phase combinatorial synthetic strategies for the quinoxaline, quinazoline and benzimidazole based privileged structures. Mini-Rev Med Chem 6:71–89. https://doi.org/10.2174/138955706775197839

Kershaw NM, Wright GSA, Sharma R et al. (2013) X-ray crystallography and computational docking for the detection and development of protein–ligand interactions. Curr Med Chem 20:569–575. https://doi.org/10.2174/0929867311320040008

Khan I, Ibrar A, Ahmed W, Saeed A (2015) Synthetic approaches, functionalization and therapeutic potential of quinazoline and quinazolinone skeletons: the advances continue. Eur J Med Chem 90:124–169. https://doi.org/10.1016/J.EJMECH.2014.10.084

Kocisko DA, Baron GS, Rubenstein R et al. (2003) New inhibitors of scrapie-associated prion protein formation in a library of 2000 drugs and natural products. J Virol. https://doi.org/10.1128/JVI.77.19.10288

Kocisko DA, Come JH, Priola SA et al. (1994) Cell-free formation of protease-resistant prion protein. Nature. https://doi.org/10.1038/370471a0

Kuwata K, Nishida N, Matsumoto T et al. (2007) Hot spots in prion protein for pathogenic conversion. Proc Natl Acad Sci USA 104:11921–11926. https://doi.org/10.1073/pnas.0702671104

Langella E, Improta R, Barone V (2004) Checking the pH-induced conformational transition of prion protein by molecular dynamics simulations: effect of protonation of histidine residues. Biophys J 87:3623–3632. https://doi.org/10.1529/BIOPHYSJ.104.043448

Langella E, Improta R, Crescenzi O, Barone V (2006) Assessing the acid-base and conformational properties of histidine residues in human prion protein (125-228) by means of pKa calculations and molecular dynamics simulations. Proteins Struct Funct Bioinforma 64:167–177. https://doi.org/10.1002/prot.20979

Linden R (2017) The biological function of the prion protein: a cell surface scaffold of signaling modules. Front Mol Neurosci 10:1–19. https://doi.org/10.3389/fnmol.2017.00077

Macedo B, Cordeiro Y (2017) Unraveling prion protein interactions with aptamers and other PrP-binding nucleic acids. Int J Mol Sci 18:1023. https://doi.org/10.3390/ijms18051023

Macedo B, Kaschula CH, Hunter R et al. (2010) Synthesis and anti-prion activity evaluation of aminoquinoline analogues. Eur J Med Chem 45:5468–5473. https://doi.org/10.1016/j.ejmech.2010.07.054

Malevanets A, Chong PA, Hansen DF et al. (2017) Interplay of buried histidine protonation and protein stability in prion misfolding. Sci Rep 7:882. https://doi.org/10.1038/s41598-017-00954-7

Mallikarjuna SM, Sandeepa C, Padmashali B (2016) Synthesis, antimicrobial activity of piperazin-1-yl (3,4,5-trimethoxyphenyl) methanone derivatives. Der Pharma Chem 8:262–268

Morris GM, Huey R, Lindstrom W et al. (2009) AutoDock4 and AutoDockTools4: automated docking with selective receptor flexibility. J Comput Chem 30:2785–2791. https://doi.org/10.1002/jcc.21256

Orru CD, Groveman BR, Hughson AG et al. (2017) RT-QuIC assays for prion disease detection and diagnostics. Methods Mol Biol 1658:185–203. https://doi.org/10.1016/B978-0-12-800946-8.00031-3

Otto M, Cepek L, Ratzka P et al. (2004) Efficacy of flupirtine on cognitive function in patients with CJD: a double-blind study. Neurology 62:714–718. https://doi.org/10.1212/01.WNL.0000113764.35026.EF

Prusiner SB (1998) Prions. Proc Natl Acad Sci USA 95:13363–13383. https://doi.org/10.1073/pnas.95.23.13363

Sashidhara KV, Kumar M, Modukuri RK et al. (2012) Antiplasmodial activity of novel keto-enamine chalcone-chloroquine based hybrid pharmacophores. Bioorg Med Chem 20:2971–2981. https://doi.org/10.1016/j.bmc.2012.03.011

Schmitz M, Cramm M, Llorens F et al. (2016) Application of an in vitro-amplification assay as a novel pre-screening test for compounds inhibiting the aggregation of prion protein scrapie. Sci Rep 6:28711. https://doi.org/10.1038/srep28711

Supattapone S (2014) Synthesis of high titer infectious prions with cofactor molecules. J Biol Chem 289:19850–19854. https://doi.org/10.1074/jbc.R113.511329

Trivedi MK, Branton A, Trivedi D, Nayak G (2016) Determination of isotopic abundance of 13C/12C or 2H/1H and 18O/16O in biofield energy treated 1-chloro-3-nitrobenzene (3-CNB) using gas chromatography-mass spectrometry. Sci J Anal Chem 4:42–51. https://doi.org/10.11648/j.sjac.20160404.11

Vieira TCRG, Cordeiro Y, Caughey B, Silva JL (2014) Heparin binding confers prion stability and impairs its aggregation. FASEB J 28:2667–2676. https://doi.org/10.1096/fj.13-246777

Waiker DK, Karthikeyan C, Poongavanam V et al. (2014) Synthesis, biological evaluation and molecular modelling studies of 4-anilinoquinazoline derivatives as protein kinase inhibitors. Bioorg Med Chem 22:1909–1915. https://doi.org/10.1016/j.bmc.2014.01.044

Westergard L, Christensen HM, Harris DA (2007) The cellular prion protein (PrPC): its physiological function and role in disease. Biochim Biophys Acta 1772:629–644. https://doi.org/10.1016/j.bbadis.2007.02.011

Wilham JM, Orrú CD, Bessen RA et al. (2010) Rapid end-point quantitation of prion seeding activity with sensitivity comparable to bioassays. PLoS Pathog 6:e1001217. https://doi.org/10.1371/journal.ppat.1001217

Yamamoto N, Kuwata K (2009) Regulating the conformation of prion protein through ligand binding. J Phys Chem B 113:12853–12856. https://doi.org/10.1021/jp905572w